DOI 10.5012/bkcs.2010.31.02.344

TiO_2/Carbon Composites Prepared from Rice Husk and the Removal of Bisphenol A in Photocatalytic Liquid System

Jiyeon Kim, Byeong Sub Kwak, and Misook Kang*

Department of Chemistry, College of Science, Yeungnam University, Gyeongsan, Gyeongbuk 712-749, Korea
**E-mail: mskang@ynu.ac.kr*
Received September 29, 2009, Accepted December 17, 2009

The improved photocatalytic performance of a carbon/TiO_2 composite was studied for the Bisphenol A (BPA) decomposition. Titanium tetraisopropoxide (TTIP) and a rice husk from Korea were heterogeneously mixed as the titanium and carbon sources, respectively, for 3 h at room temperature, and then thermally treated at 600 ^oC for 1 h in H_2 gas. The transmission electron microscopy (TEM) images revealed that the bulk carbon partially covered the TiO_2 particles, and the amount that was covered increased with the addition of the rice husk. The acquired carbon/TiO_2 composite exhibited an anatase structure and a novel peak at $2\theta = 32^o$, which was assigned to bulk carbon. The specific surface area was significantly enhanced to 123 ~ 164 m^2/g in the carbon/TiO_2 composite, compared to 32.43 m^2/g for the pure TiO_2. The X-ray photoelectron spectroscopy (XPS) results showed that the Ti-O bond was weaker in the carbon/TiO_2 composite than in the pure TiO_2, resulting in an easier electron transition from the Ti valence band to the conduction band. The carbon/TiO_2 composite absorbed over the whole UV-visible range, whereas the absorption band in the pure TiO_2 was only observed in the UV range. These results agreed well with an electrostatic force microscopy (EFM) study that showed that the electrons were rapidly transferred to the surface of the carbon/TiO_2 composite compared to the pure TiO_2. The photocatalytic performance of the BPA removal was optimized at a Ti:C ratio of 9.5:0.5, and this photocatalytic composite completely decomposed 10.0 ppm BPA after 210 min, whereas the pure TiO_2 achieved no more than 50% decomposition under any conditions.

Key Words: Carbon/TiO_2 composites, Rice husk in Korea, Removal of Bisphenol A, Photocatalysis

Introduction

Bisphenol A (BPA) is manufactured in high quantities, and 90% of BPA that is produced is used as a monomer for the production of polycarbonate and epoxy resins, unsaturated polyester-styrene resins, and flame retardants. These final products are used as can coatings, powdered paints, thermal paper additives, dental fillings, and antioxidants in plastics.

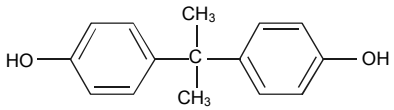

Bisphenol A

BPA exhibits an estrogenic activity and is considered an environmental endocrine disrupter.[1] Moreover, BPA has been reported to leach from polycarbonate baby bottles,[2] reusable containers,[3] and drinking water tanks.[4] BPA has also been detected in plastic waste,[5] plasma stored in polycarbonate tubes,[6] and in aquatic environments.[7] High concentrations of BPA can also be present in wastewater from BPA production factories because BPA is only partially removed during the wastewater treatment, and the wastewater containing BPA is a source of contamination in aquatic environments.[8] Although BPA is readily degraded by microorganisms, the biological methods that are used to treat wastewater containing high concentrations of BPA commonly require long treatment times. Therefore, a rapid and simple wastewater treatment method for BPA is urgently required. Various techniques involving chemical,[9] biological,[6,10] photochemical,[11] and electrochemical[7] procedures have been studied for the treatment of wastewater that contains phenolic compounds. Recently, several researchers have examined the photocatalytic treatment of BPA-containing wastewater through the degradation of BPA in the presence of TiO_2 as a photocatalyst.

Lee *et al.*[12] used immobilized TiO_2 particles for the photodegradation BPA, where the titanium sol solution that synthesized using a sol-gel method was used as a binder. They also investigated the effects of various parameters, such as the film thickness, the UV radiation intensity, and the pH, on the photodegradation. Kang *et al.*[13] also reported that alkali metal-TiO_2 particles have an anatase structure and were *ca.* 50 - 100 nm in size with a surface area of ca. 14 ~ 24 m^2/g. K-TiO_2 photocatalysis was used to completely degrade 10.0 ppm BPA after 50 h. Serpone *et al.*[14] examined the microwave-assisted photodegradation of BPA in the presence of TiO_2. The photo-activity of the titanium dioxide particles was somehow promoted by the microwave radiation. Tsai *et al.*[15] suggested that the photocatalytic degradation of BPA in the TiO_2 suspension process is an efficient method for quickly lowering the concentration of the endocrine disrupting compound in water. Additionally, many groups have recently tried other metal semiconductors in the photocatalysis.[16,17] Despite these research efforts, the photodecomposition of macro molecules containing an aromatic ring such as BPA is still difficult. Therefore, further research on these improved materials is necessary. Particularly, the development of a photocatalyst that simultaneously possesses high adsorption and decomposition abilities would greatly improve the decomposition performance. In this study, bulk carbon was selected as the high

surface area material in order to achieve a high adsorption ability was achieved for macro organic molecules, similar to BPA. Rice husk that was harvested in South Korea was used as the carbon source because of its low cost and waste recycling capability.

In this study, the TiO_2 photocatalysts were prepared using a heterogeneous mixture of titanium tetraisopropoxide (TTIP) and rice husk for Korea as the titanium and carbon sources, respectively, with thermal treatment at 600 °C in H_2 gases, and bulk carbon partially covered these photocatalysts. Then the TiO_2 photocatalysts were used to photodecompose BPA (10.0 ppm). The adsorption effects, structural variations, surface state, and elemental compositions were investigated four different carbon/TiO_2 composites. The chemical and morphological structure of the carbon/TiO_2 composites was studied using the Brunauer, Emmett and Teller (BET) surface area, X-ray diffraction (XRD), transmission electron microscopy (TEM), electrostatic force microscopy (EFM), and energy dispersive X-ray (EDX) analysis. Finally, the BPA solutions that were obtained from the photolysis and electrolysis with the carbon/TiO_2 system were characterized using a UV/vis spectrophotometer.

Experimental

Carbon/TiO_2 catalyst preparation. A conventional impregnation method was used to prepare the carbon/TiO_2 photocatalyst. TTIP (99.95%, Junsei Chemical, Japan) and a rice husk (Jeju, Korea) were used as the titanium dioxide and carbon precursors, respectively. The rice husk was finely grated to about 25 - 30 mesh before the mixing step. The concentrations of Ti and carbon varied in the range of 9.5:0.5, 9.0:1.0, 8.5:1.5, and 7.0:3.0 for 1.0 mol % per TTIP in the initial solution. Distilled water was used as the solvent for the hydrolysis. A mixed solution of the TTIP and rice husk precursors, acetic acid (Junsei Chemical Co. Ltd., Japan), and distilled water was stirred for 3 h until a homogeneous gel formed. The water was evaporated out at 80 °C for 3 h. The damped precipitate was dried and calcined at 100 °C for 24 h and at 600 °C for 2 h in a 9.0 N_2/1.0 H_2 mixed gas.

Carbon/TiO_2 catalysts characterization. The synthesized carbon/TiO_2 powders were examined using XRD (X-ray diffractometer, MPD, PANalytical, Yeungnam University, Korea) with nickel-filtered CuKα radiation (30 kV, 30 mA) at 2θ angles ranging from 10 to 75°, a scan speed of 10° min^{-1} and a time constant of 1 s. The sizes and shapes of the carbon/TiO_2 particles were measured using TEM (Transmittance Electron Microscopy, H-7600, Hitachi, Yeungnam University, Korea) that was operated at 120 kV.

The BET surface areas and the pore volume of the powders were measured through nitrogen gas adsorption using a continuous flow method using a chromatograph (Metrics Gemini 2375, Londonderry, Yeungnam University, Korea) that was equipped with a thermal conductivity detector (TCD) at a liquid-nitrogen temperature. A mixture of nitrogen and helium was used as the carrier gas, and the sample was treated at 350 °C for 1 h before the nitrogen adsorption.

The X-ray photoelectron spectroscopy (XPS; Cooperative Center to Research Facilities, Sungkyunkwan University Instrumental Analysis Center, Korea) measurements of Ti2p, C1s, Si2p, and O1s were recorded using an ESCA 2000 (VZ Micro-Tech, Oxford, UK) system that was equipped with a non-monochromatic AlKα (1486.6 eV) X-ray source. The base pressure of the ESCA system was below 1×10^{-9} Pa. The reflectance UV-visible spectra were obtained using a Cary 500 spectrometer with a reflectance sphere over the special range of 200 to 800 nm. The surface states and electric properties of the carbon/TiO_2 film were determined using EFM (resolution; 0.1 nm (X- Y), 0.01 nm (Z), Dimension3100, Veeco Co., National Center for Nanomaterials Technology, Pohang, Korea).

Photodecomposition of Bisphenol A. BPA (97%, Sigma-Aldrich Korea LTD) was decomposed using a general stationary apparatus. The initial BPA concentration was fixed at 10.0 ppm. First, BPA was dissolved at a concentration of 10.0 ppm in water and then diluted with a 1.0-liter aqueous solution. The carbon/TiO_2 powders were directly used for the BPA photodecomposition reaction. The UV lamps (model UV-A, 365 nm, 6 W × 3 ea, 20 cm length × 1.5 cm diameter, Shinan Co., Korea) were equipped with a photocatalytic liquid system, and the photocatalyst concentration was 0.5g/1.0 L. The BPA concentration was analyzed before and after the reaction using UV-visible spectroscopy (Shimadzu MPS-2000 spectrometer).

Results and Discussion

Physical characterizations of the pure TiO_2 and carbon/TiO_2 photocatalysts. Figure 1 shows the XRD patterns of the pure TiO_2 and carbon/TiO_2 photocatalysts with Ti:C ratios of 9.5:0.5, 9.0:1.0, 8.5:1.5, and 7.0:3.0. All of the samples exhibited a perfectly anatase structure, and the peaks at 25.3, 38.0, 48.2, 54, 63, and 68° 2θ were assigned to the (d_{101}), (d_{004}), (d_{200}), (d_{105}), (d_{211}), and (d_{204}) planes, respectively.[18] The line broadening of the [101] peak was related to the size of the hexagonal crystalline phase of titania. The crystalline domain size was using the Scherrer's equation, τ (crystalline domain size) = 0.9λ / βcosθ,

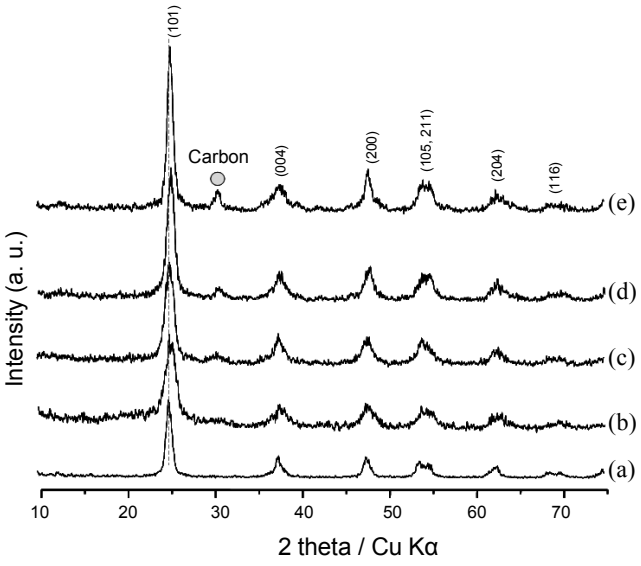

Figure 1. XRD patterns of the pure TiO_2 and carbon/TiO_2 photocatalysts with various Ti:C ratios: (a) pure TiO_2 (sol-gel method), (b) 0.5C:9.5Ti, (c) 1.0C:9.0Ti, (d) 1.5C:8.5Ti, and (e) 3.0C:7.0Ti.

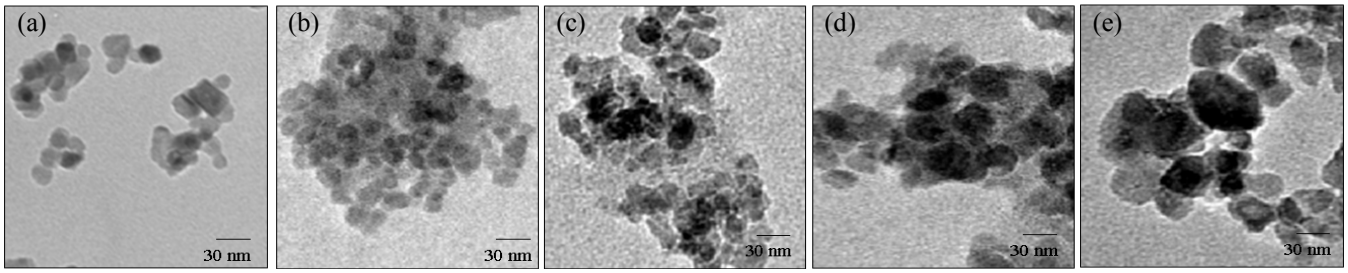

Figure 2. TEM images of the particle shapes of the pure TiO_2 and carbon/TiO_2 photocatalysts with various Ti:C ratios: (a) pure TiO_2 (sol-gel method), (b) 0.5C:9.5Ti, (c) 1.0C:9.0Ti, (d) 1.5C:8.5Ti, and (e) 3.0C:7.0Ti.

Table 1. Specific surface area and real atomic composition of the carbon/TiO_2 powders: (a) pure TiO_2 (sol-gel method), (b) 0.5C:9.5Ti, (c) 1.0C:9.0Ti, (d) 1.5C:8.5Ti, and (e) 3.0C:7.0Ti.

(A) Atomic compositions

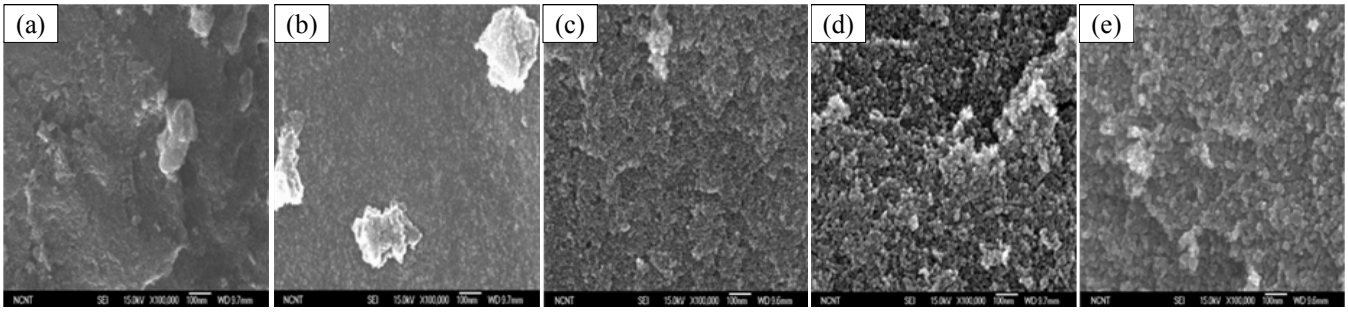

Element	Weight %	Atomic %
OK	47.96	81.94
TiK	31.59	18.03

Element	Weight %	Atomic %
CK	37.10	51.56
OK	37.96	39.60
SiK	0.65	0.38
TiK	24.29	8.46

Element	Weight %	Atomic %
CK	47.13	62.03
OK	30.92	30.55
SiK	0.76	0.43
TiK	21.19	6.99

Element	Weight %	Atomic %
CK	28.76	42.94
OK	40.17	45.02
SiK	1.56	0.99
TiK	29.51	11.04

Element	Weight %	Atomic %
CK	25.87	39.37
OK	40.90	46.73
SiK	4.53	2.95
TiK	28.69	10.95

(B) Surface areas and pore volumes

Samples	BET Multipoint Surface Area (m^2/g)	BET Single Point Surface Area (m^2/g)	Langmuir Surface (m^2/g)	Adsorption total pore volume at p/p_0 (cc/g)
e) Ti/C (7.0:3.0)	144.3056	144.2964	218.6804	0.0733
d) Ti/C (8.5:1.5)	164.4525	162.8441	253.5862	0.0827
c) Ti/C (9.0:1.0)	148.9769	147.2393	230.4333	0.0748
b) Ti/C (9.5:0.5)	123.8709	122.1646	192.2262	0.0621
a) TiO_2 (sol-gel)	32.43	31.65	37.56	3.56

where λ is the wavelength of the incident X-rays, β is the full width at the half maximum height in radians, and θ is the diffraction angle. The estimated crystalline domain sizes were 26.3, 26.1, 29.2, 30.7 and 40.7 nm for the Ti:C concentration ratios of 10.0:0.0, 9.5:0.5, 9.0:1.0, 8.5:1.5, and 7.0:3.0, respectively. Additionally, all of the peaks shifted to high values of 2θ because of the partial incorporation of carbon into the TiO_2 anatase framework. This tendency was distinguishable through the increase in the carbon concentration. A peak that was assigned to bulk carbon (e.g. at 31° of 2θ) appeared when carbon was mixed into TiO_2, indicating that the bulk carbon covered the TiO_2 surface.

Figure 2 shows the TEM images of the particle shapes of the pure TiO_2 and carbon/TiO_2 photocatalysts with Ti:C ratios of 9.5:0.5, 9.0:1.0, 8.5:1.5, and 7.0:3.0. A relatively uniform mixture of rhombic and cubic particles was observed in the pure TiO_2 with an approximate size of 20 nm. As carbon was added, the bulk carbon more completely covered the TiO_2 particles, except for 0.5 carbon/9.5 TiO_2, in the order of pure 0.5 carbon/9.5 TiO_2 < TiO_2 < 1.0 carbon/9.0 TiO_2 < 1.5 carbon/8.5 TiO_2 < 3.0 carbon/7.0 TiO_2. The surfaces of these composites were blackened with increasing carbon content. These result confirmed that the bulk carbon that was prepared from the rice husk evenly covered the external surface of the TiO_2 nano-sized particles rather than growing as separate particles.

Table 1 summarizes the specific surface area and the real atomic composition of the carbon/TiO_2 powders. The pure TiO_2 and the 0.5 carbon/0.95 TiO_2 composite were not porous. How-

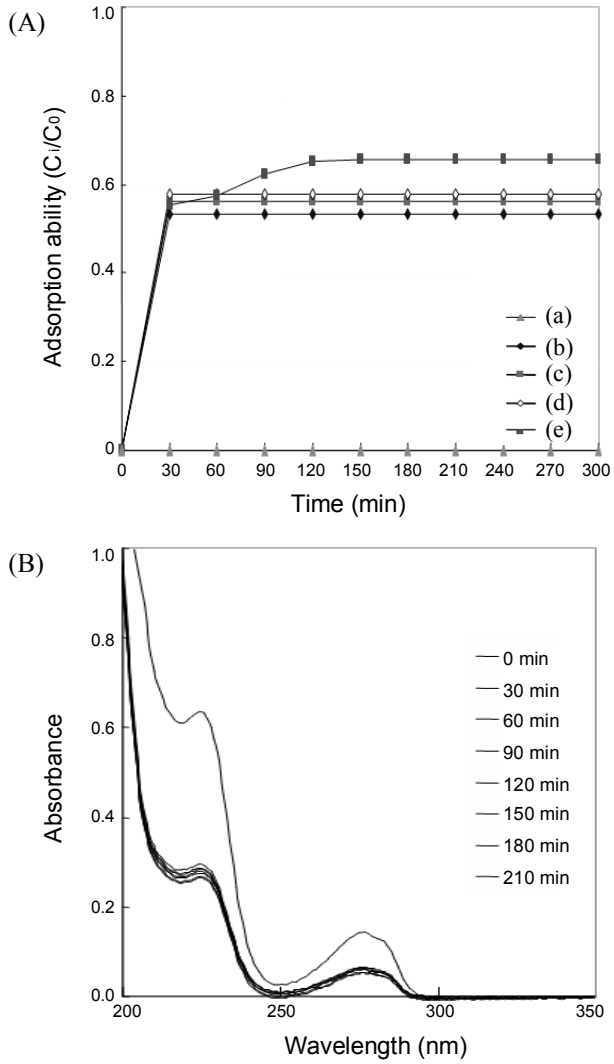

Figure 3. Comparison of the (A) absorption ability for BPA on the pure TiO_2 and carbon/TiO_2 photocatalysts and the (B) change of UV-visible spectrum for BPA over Ti/C(9.5:0.5): (a) pure TiO_2 (sol-gel method), (b) 0.5C:9.5Ti, (c) 1.0C:9.0Ti, (d) 1.5C:8.5Ti, and (e) 3.0C:7.0Ti. Reaction conditions: 2.0 L liquid system, room temp.; BPA concentration, 10 ppm; catalyst amount, 0.5g/1.0L.

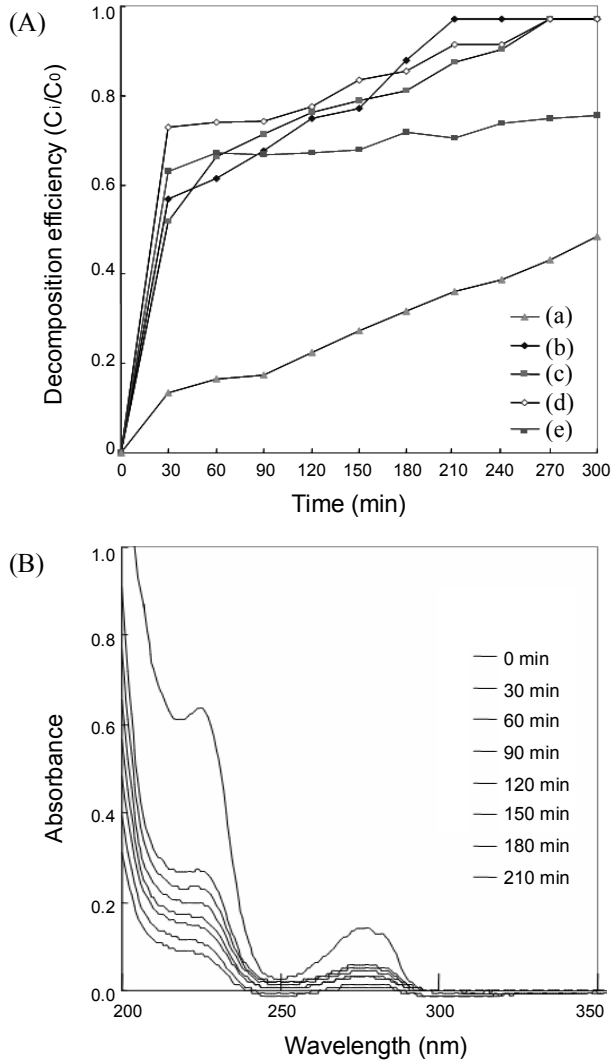

Figure 4. The (A) photocatalytic performance for the BPA decomposition on the pure TiO_2 and carbon/TiO_2 photocatalysts and the (B) change of UV-visible spectrum for BPA over Ti/C(9.5:0.5): (a) pure TiO_2 (sol-gel method), (b) 0.5C:9.5Ti, (c) 1.0C:9.0Ti, (d) 1.5C:8.5Ti, and (e) 3.0C:7.0Ti. Reaction conditions: 2.0 L liquid system, room temp.; light sorce, UV-A (365 nm, 6W × 3ea); BPA concentration, 10 ppm; catalyst amount, 0.5g/1.0L.

ever, uniformly pores without any TiO_2 lumps were observed when carbon was added, and the pore size increased with increasing carbon amount. The maximum amount of deposited carbon was observed for the 1.0 carbon/9.0 TiO_2 composite, but the minimum value occurred for the 1.5 - 3.0 carbon / 0.95 - 0.7 TiO_2 composites because the carbon eventually covered the entire surface of both the SiO_2 in the rice husk and the TiO_2, and the amount of deposited carbon was considerably small. The amount SiO_2 that was produced increased through the addition of the rice husk. Generally, surface area relative to the volume is strongly related to the particle size, and the surface area increases with decreasing particle size. However, these results showed the opposite tend, where the BET surface area of 164.4 m^2/g was excellent for 1.5 carbon/0.85 TiO_2 compared to a value of 32.43 m^2/g for TiO_2. The pore volume exhibited the same trend because the blanket of carbon between the neutrally charged carbon/TiO_2 particles led to an increase in the bulk porosity. Otherwise, the charged TiO_2 particles on the surface induced the particle coagulation, thereby reducing the porosity.

Photodecomposition of BPA for the pure TiO_2 and carbon/TiO_2 photocatalyst. Figure 3 shows the absorption ability of BPA on the pure TiO_2 and carbon/TiO_2 photocatalysts. The BPA concentration was determined using a UV-visible spectrometer, in the right-hand figure, and the two absorption bands at 220 and 280 nm were induced by the aromatic ring. The carbon-coated catalysts were more absorbent to BPA because the carbon had a large specific surface area due to the bulk pores. However, over time, the absorption process stopped, and the concentration of the BPA in the reactor did not change, At this point, the UV-visible absorption was constant. However BPA did not adsorb to the TiO_2 nanoparticles, because the pure TiO_2 did not contain pores and hence had a very small specific surface area. Most

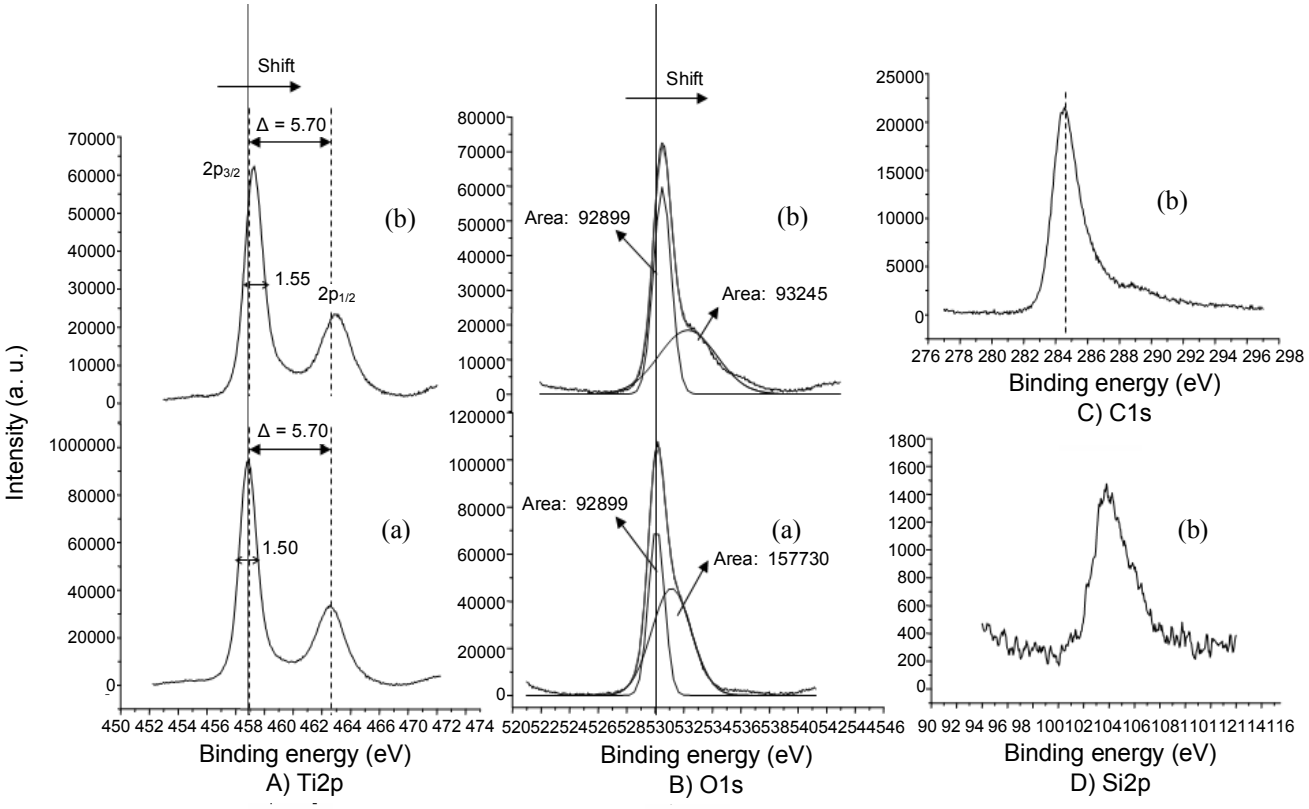

Figure 5. Quantitative XPS analysis of the (a) pure TiO_2 and (b) 0.5 carbon/9.5 TiO_2 particles: A) Ti2p, B) O1s, C) C1s, and D) Si2p.

notably, 67% of the BPA was absorbed on the 0.5 carbon/9.5 TiO_2 composite after 120 min compared to 0% on the pure TiO_2. As predicted in the introduction, the absorption capability increased with increasing carbon content in the following order: TiO_2 < 0.5 carbon/9.5 TiO_2 < 1.0 carbon/9.0 TiO_2 < 1.5 carbon/8.5 TiO_2 < 3.0 carbon/7.0 TiO_2 because of the large surface area of carbon.

Figure 4 shows the photocatalytic performance of the BPA decomposition for the pure TiO_2 and carbon/TiO_2 photocatalysts. The photodecomposition of BPA increased through the addition of carbon, and the increased absorption was particular fast after the initial carbon addition. BPA was perfectly decomposed in the UV-A radiation/air bubbling/0.5 carbon/9.5 TiO_2 photocatalytic system after 210 min (3.5 h). As previously reported,[13] 10.0 ppm BPA was decomposed after 52 hours in pure TiO_2. However, in this present study, 49% of the 5.0 ppm BPA was photodecomposed in the pure TiO_2 system after 5 hours, which was an improvement over the previous results. In this study, the pure TiO_2 was reduced by hydrogen gas before the photocatalytic reaction of Bisphenol A. This process was expected to change the oxidation state of the pure TiO_2 from 4 to 3, and this affected the band gap, resulting in the change in the photocatalytic activity. Consequently, the reduction process appeared to improve the active photocatalyst. In particular, the present data results for the carbon/TiO_2 composites were very encouraging. Additionally, 5.0 ppm BPA was completely decomposed after 30 min in the 0.5 carbon/9.5 TiO_2 photocatalytic system, but 15.0 ppm BPA was only 75% decomposed even after 300 minutes. The BPA absorption band in the UV-visible spectrum was consistently small over the photo oxidative reaction time. Therefore, the bulk carbon, with a high surface area, exerted a synergistic effect on the photocatalytic performance of the carbon/TiO_2 composite for the BPA decomposition.

Comparison of optical property on the pure TiO_2 and carbon/TiO_2 photocatalyst. The quantitative XPS analysis was performed on the pure TiO_2 and the 0.5 carbon/9.5 TiO_2 particles, which was selected as the representative carbon/TiO_2 catalyst. Figure 5 shows the typical survey and high-resolution spectra. The survey spectra of the pure TiO_2 and carbon/TiO_2 particles contained Ti2p, C1s, Si2p, and O1s peaks. The $Ti2p_{1/2}$ and $Ti2p_{3/2}$ spin-orbital splitting photoelectrons of the the two samples were located at binding energies of 464.7 eV and 458.5 eV, respectively. The binding energy was not expected to decrease after carbon was added. In general, an increase in the binding energy corresponds to an increase in the oxidation state of the metal.[19] The titanium oxidation state in the carbon/TiO_2 (maybe Ti^{5+}) composite was higher than the Ti^{4+} state in the pure TiO_2. The activity of the Ti photocatalysts was closely related to the Ti oxidation states. Generally, the O1s region is decomposed into several contributions. The Gaussian values were used in the curve resolution of the two individual O1s peaks (first peak O1: 530 - 531.0 eV, second peak O2: 532 - 533.0 eV) in the two spectra, and these peaks were assigned to Ti-O and Ti-OH, respectively. The location of the binding energies for the second peak agreed well with the reported values for the bulk oxide (O^{2-}) and the hydroxyl (OH) species. However, the second peak separation in the pure TiO_2 was not clear. These results were tentatively attributed to the different oxidation state of the bulk oxygen because

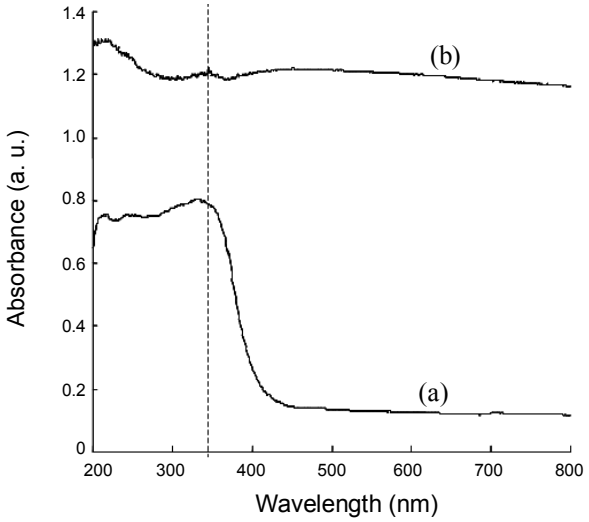

Figure 6. UV-visible spectra of the (a) pure TiO_2 and (b) 0.5 carbon/9.5 TiO_2 particles.

otherwise the peak at 533.0 eV would be perfectly divided from the first peak at 530.0 eV in the carbon/TiO_2 composite. In general, a large hydroxyl (OH) species peak indicates a high hydrophilicity,[20] and many OH radicals are produced in the holes of the valence band, thereby improving the photocatalytic performance. These results indicated that the Ti-OH bonding strength was weaker in the carbon/TiO_2 composite than in the pure TiO_2, from the hard soft acid base (HSAB) rule, resulting in an easier electron flow on the external surface of TiO_2. On the other hand, the C1s peak at 284.6 eV and the Si2p peak at 104.0 eV were both observed in the carbon/TiO_2 sample because the rice husk was composed of 20 wt % Si and 80 wt % carbon.

The UV-visible spectra of the pure TiO_2 and the 0.5 carbon/9.5 TiO_2 particles, which was selected as the representative carbon/TiO_2 catalyst, were obtained in order to determine the relationship between the photocatalytic performance and the spectroscopic properties, in Figure 6. The absorption band corresponding to the tetrahedral symmetry of Ti^{4+} normally appears at approximately 350 nm and is assigned to the ligand (p-orbital, oxygen) to ligand (s, p-orbital, oxygen) charge transfer. The band gaps of a semiconductor material are closely related to the wavelength range that is absorbed, and the band gap decreases with increasing absorption wavelength. Remarkably, the 0.5 carbon/9.5 TiO_2 composited absorbed the entire spectra across the complete UV and visible range because of the ligand (p-orbital, carbon) to metal (d-orbital, Ti) charge transfer and the d-d transfer of the metal that occurred when an electron existed in the d-orbital of Ti. Therefore, the complete carbon coverage of the TiO_2 surface facilitated the electron transfer despite the weak radiation, suggesting that the electron transfer activities were eased on the surface of the carbon/TiO_2 composite.

The analytical EFM method was used in order to determine if the surface of electrode was flat because good electron flow is induced by a flat electrode surface. Typically, the presence of a conductor and non-conductor within a nanometer-leveled film can be distinguished using atomic force microscopy (AFM) for the modified EFM image. The power strength of the image between the samples and tips was measured while traversing the voltage to the AFM tip bias. The presence of the conducting and non-conducting areas in the sample can be determined from the responses of the AFM tip.[21] The phase periodically changed with the tip vibrating power cycle (charge, magnetic, *etc.*). Consequently, the differences between the conducting and non-conducting surfaces were indicated by the amplitude and phase changes, and the change in the width was expressed by the contrast in the images and the roughness values (Ra). The Ra value can indirectly be determined by changing the twitch of the tip using the following equation:[22,23]

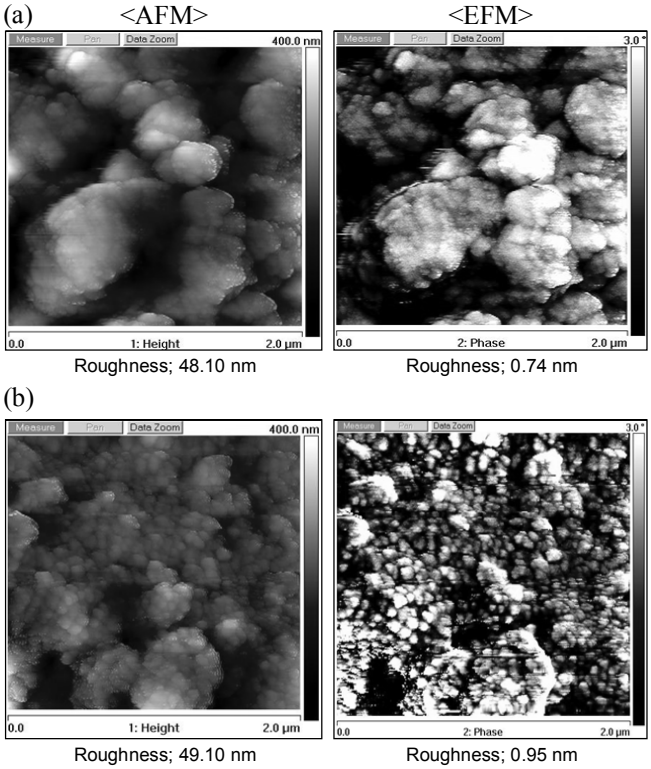

Figure 7. EFM images of the (a) pure TiO_2 and (b) 0.5 carbon/9.5 TiO_2 particles in light.

$$Ra = 1/L_x L_y \int_0^{L_y} \int_0^{L_y} \left| f(x, y) \right| dx\, dy$$

In this equation, f(x, y) is the surface relative to the center plane, and L_x and L_y are the dimensions of the surface. Figure 7 shows the EFM images of the pure TiO_2 and the 0.5 carbon/9.5 TiO_2 particles, which was used as the representative carbon/TiO_2 catalyst, in light. A voltage of 3.0 eV was traversed, and 2.0-μm-thick film samples were used. The phase change did not exceed 3.0 degrees in either sample. The phase difference is the difference in the electrostatic force between phases, and therefore, a bright image generally indicates the flow of charge[24]: As the current passes through the sample, a bright phase is exhibited if the generated electromagnetic spectra undergo reinforcing interference, whereas a dark phase is observed for offset interference. The brightness of both samples increased in light condition compared to in the darkroom. The carbon/TiO_2 com-

posite exhibited a better brightness in light than the pure TiO_2. The value at the bottom of the figure indicates the averaged Ra values of the two samples in light. The carbon/TiO_2 composite was significantly more uniform than the pure TiO_2 and exhibited a higher Ra value of 0.95 degrees in light. Therefore, the electrons flowing on the surface of the carbon/TiO_2 composite exhibited a good mobility.

Conclusions

In this study, carbon/TiO_2 composites were fabricated and characterized. The adsorption ability, the surface properties, and the chemical composition of the carbon/TiO_2 composites were investigated. The surface areas and pore volumes of the carbon/TiO_2 samples markedly increased with increasing carbon content. The TEM results revealed that the bulk carbon uniformly covered the nanometer-sized sample particles. The 0.5 carbon/9.5 TiO_2 composite absorbed the entire spectra across the complete UV and visible range because of the ligand (p-orbital, carbon) to metal (d-orbital, Ti) charge transfer and the d-d transfer of the metal that occurred when an electron existed in the d-orbital of Ti. According the hard and soft acid and base (HSAB) rule, the XPS results indicated that the Ti-OH bonding strength was weaker in the carbon/TiO_2 composite than in the pure TiO_2, resulting in easier electron flow on the external surface of TiO_2. The carbon/TiO_2 composite was significantly more uniform than the pure TiO_2, and the composite exhibited a higher Ra value of 0.95 degrees in light, from the EFM images. Therefore, the electrons that flowed on the surface of the carbon/TiO_2 composite exhibited a good mobility. The photocatalytic results for the UV-decomposition of BPA with the carbon/TiO_2 composites showed that the 0.5 carbon/9.5 TiO_2 photocatalytic composite exhibited an excellent degradation effect with respect to the reaction time because of the increased electron mobility and OH radical generation. The BPA decomposition in the aqueous solution occurred because of the synergistic effect between the photodecomposition and the absorption efficiency through carbon-photocatalysis.

Acknowledgments. This research was supported by a Yeungnam University research grant, No.209-A-380-103, and the authors are very grateful for this support.

References

1. Krishnan, A. V.; Starhis, P.; Permuth, S. F.; Tokes, L.; Feldman, D. *Endocrinology* **2004**, *132*, 2279.
2. Mountfort, K. A.; Kelly, J.; Jickells, S. M.; Castle, L. *Food Addit. Contam.* **1997**, *14*, 737.
3. Brotons, J. A.; Olea-Serrano, M. F.; Villalobos, M.; Pedraza, V.; Olea, N. *Environ. Health Perspect.* **1995**, *103*, 608.
4. Le, H. H.; Carlson, E. M.; Chua, J. P.; Belcher, S. M. *Toxicology Lett.* **2008**, *176*, 149.
5. Chang, C.; Chou, C.; Lee, M. *Analytica Chimica Acta* **2005**, *539*, 41.
6. Kang, J.; Katayama, Y.; Kondo, F. *Toxicology* **2006**, *217*, 81.
7. Kuramitz, H.; Matsushita, M.; Tanaka, S. *Water Res.* **2004**, *38*, 2331.
8. Katsumata, H.; Kawabe, S.; Kaneco, S.; Suzuki, T.; Ohta, K. *J. Photochem. Photobiol. A* **2004**, *162*, 297.
9. Oku, A.; Tanaka, S.; Hata, S. *Polymer* **2000**, *41*, 6749.
10. Kang, J.; Kondo, F. *Chemosphere* **2002**, *49*, 493.
11. Rivaton, A.; Mailhot, B.; Soulestin, J.; Varghese, H.; Gardette, J. L. *Polym. Degrad. Stabil.* **2002**, *75*, 17.
12. Lee, J.; Kim, M.; Kim, B. *Water Res.* **2004**, *38*, 3605.
13. Yeo, M.; Kang, M. *Water Res.* **2006**, *40*, 1906.
14. Horikoshi, S.; Kajitani, M.; Serpone, N. *J. Photochem. Photobiol. A* **2007**, *188*, 1.
15. Tsai, W.; Lee M.; Su, T.; Chang, Y. *J. Hazard. Mater.* **2009**, *168*, 26.
16. Tsai, W.; Lai, C.; Su, T. *J. Hazard. Mater.* **2009**, *134*, 169.
17. Chiang, K.; Lim. T. M.; Tsen, L.; Lee, C. *Appl. Catal. A* **2004**, *261*, 225.
18. Baia, L.; Peter, A.; Cosoveanu, V.; Indrea, E.; Baia, M.; Popp, J.; Danciu, V. *Thin Solid Films* **2006**, *511*, 512.
19. Ge, L. *J. Mol. Catal. A* **2008**, *282*, 62.
20. Jeong, K. M.; Yeo, M.; Kang, M. *J. Ind. Eng. Chem.* **2008**, *14*, 396.
21. Wang, H.; Hua, M.; Liu, N.; Xiaa, M.; Kea, F.; Bai, Y. *Chem. Eng. Sci.* **2007**, *62*, 3589.
22. Henke, L.; Nagy, N.; Krull, U. J. *Biosens. Bioelectron.* **2002**, *17*, 547.
23. Arnault, J. C.; Knoll, A.; Smigiel, E.; Cornet, A. *Appl. Surf. Sci.* **2001**, *171*, 189.
24. Lei, C. H.; Das, A.; Elliott, M.; Macdonald, J. E. *Nanotechnology* **2004**, *15*, 627.